INTERNATIONAL JOURNAL FOR NUMERICAL METHODS IN FLUIDS
Int. J. Numer. Meth. Fluids 2015; **78**:63–75
Published online 29 January 2015 in Wiley Online Library (wileyonlinelibrary.com). DOI: 10.1002/fld.4007

A hybrid numerical method for the phase-field model of fluid vesicles in three-dimensional space

Jaemin Shin[1], Darae Jeong[2], Yibao Li[3], Yongho Choi[2] and Junseok Kim[2,*,†]

[1]*Institute of Mathematical Sciences, Ewha W. University, Seoul 120-750, Korea*
[2]*Department of Mathematics, Korea University, Seoul 136-713, Korea*
[3]*School of Mathematics and Statistics, Xi'an Jiaotong University, Xi'an 710049, China*

SUMMARY

We propose an accurate and robust numerical method for the phase-field model of fluid vesicles. An equilibrium shape of fluid vesicle is obtained by minimizing the bending energy with volume and surface area constraints. We propose a hybrid numerical scheme that combines the Lagrange multiplier and penalty methods for two constraints. The numerical method is based on a nonlinearly stabilized splitting scheme and a direct volume correction algorithm. A large penalty constant is generally required; however, it does not guarantee that the surface area converges to a given value. Thus, we propose an adaptive constraint algorithm for the penalty method. Various numerical examples are performed to demonstrate the accuracy and robustness of the proposed method. Copyright © 2015 John Wiley & Sons, Ltd.

Received 18 June 2014; Revised 10 November 2014; Accepted 3 January 2015

KEY WORDS: fluid vesicles; Lagrange multiplier; phase-field model; penalty method; hybrid method; multigrid method

1. INTRODUCTION

Biological vesicle membranes are complex structures whose fundamental components include lipids, proteins, and cholesterol; see Figure 1. These are widely studied in biology, biophysics, and bioengineering because the biomembranes form the basic structural units and the membrane morphology plays an important role in their biological function [1, 2].

There have been many experimental studies on the configurations and deformations of elastic biomembranes [3–6]. The equilibrium configurations of a vesicle membrane are obtained by minimizing the elastic bending energy with a prescribed volume and surface area. The constant surface area is considered by the incompressibility of the membrane. And, the constant volume is considered vesicle with the inside pressure and outside pressure balanced by the osmotic pressure [7].

The deformation of vesicle membranes was observed in a study of the elastic bending energy using a phase-field approach [8–10] and in incompressible viscous fluid [11–13]. In the other way, a dynamically triangulated membrane model has been employed to study fluid vesicles [14–16] and red blood cells [17, 18]. In [8–10, 13, 19, 20], authors have studied numerical ideas for the simulation of Willmore flow. By using Lagrange multipliers, the model in [7, 10, 20–23] can effectively incorporate constraints for preserving the volume and surface area. In [8, 13, 19, 24], the authors used penalty methods to enforce the volume and surface area constraints. In general, the methods need large penalty constants; however, it has stability and convergence problems.

Numerical experiments of fluid vesicle are important to demonstrate the real phenomenon. The surface area of fluid vesicle under specific flow conditions is usually not constant. However, the

*Correspondence to: Junseok Kim, Department of Mathematics, Korea University, Seoul 136-713, Korea.
†E-mail: cfdkim@korea.ac.kr

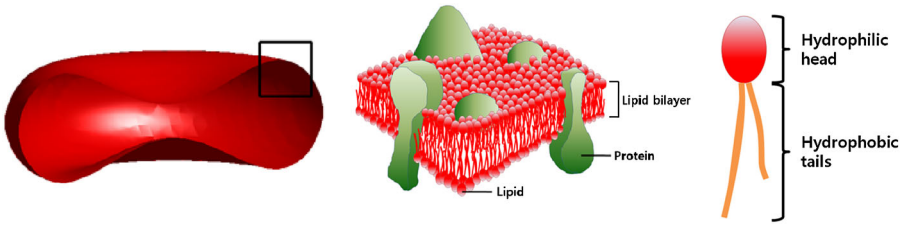

Figure 1. Schematic representation of (a) membrane, (b) lipid bilayer, and (c) single lipid.

incompressibility of the membrane restricts the flow field to have the two-dimensional divergence free on the vesicle surface. Also, the constant volume requires the flow field to be three-dimensional divergence free on the whole domain. Therefore, the fluid vesicle dynamics satisfy the volume conservation with the given surface area.

We present a numerical method for the phase-field model of the Willmore flow with the volume conservation and surface area constraint. This paper is organized as follows. In Section 2, we briefly review the Lagrange multiplier and the penalty methods and propose a hybrid method. We describe the numerical method for the Willmore flow and the adaptive method for the surface area constraint in Section 3. Numerical experiments are presented in Section 4, and conclusions are given in Section 5.

2. PHASE-FIELD MODEL FOR A VESICLE MEMBRANE

The equilibrium shape of a vesicle membrane Γ is determined by minimizing the bending energy [25, 26]

$$\mathcal{E}_{\text{elastic}} = \int_{\Gamma} \kappa H^2 ds, \tag{1}$$

where κ is the bending rigidity and H is the mean curvature of the membrane surface. A phase-field function $\phi(\mathbf{x})$ is defined in the computational domain Ω to represent the vesicle membrane as $\Gamma = \{\mathbf{x} : \phi(\mathbf{x}) = 0\}$, the inside of the membrane as $\{\mathbf{x} : \phi(\mathbf{x}) > 0\}$, and the outside of the membrane as $\{\mathbf{x} : \phi(\mathbf{x}) < 0\}$; see Figure 2. The regions away from the membrane Γ are close to $\phi = 1$ or -1.

We assume that the phase-field function is a hyperbolic tangent profile as

$$\phi(r) = \tanh\left(\frac{r}{\sqrt{2}\epsilon}\right), \tag{2}$$

where r is a local coordinate along the interface normal. A transition parameter ϵ is taken to be a finite but small positive value. We then have the equality

$$F(\phi) = \frac{(\phi^2 - 1)^2}{4} = \frac{\epsilon^2}{2}|\nabla\phi|^2. \tag{3}$$

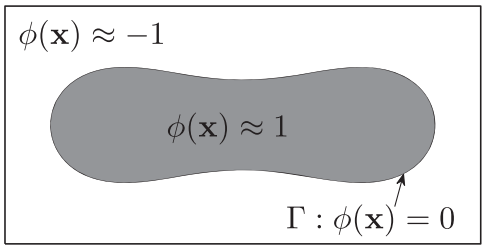

Figure 2. Schematic illustration of phase-field function for a vesicle membrane.

DOI: 10.1002/fld

The mean curvature is defined as $H = \nabla \cdot (\nabla\phi/|\nabla\phi|)$, and it can be expanded as

$$\begin{aligned} H &= \nabla\left(\frac{1}{|\nabla\phi|}\right)\cdot\nabla\phi + \frac{\Delta\phi}{|\nabla\phi|} = \nabla\left(\frac{\sqrt{2}\epsilon}{1-\phi^2}\right)\cdot\nabla\phi + \frac{\Delta\phi}{|\nabla\phi|} \\ &= \frac{2\sqrt{2}\epsilon\phi|\nabla\phi|^2}{(1-\phi^2)^2} + \frac{\Delta\phi}{|\nabla\phi|} = \frac{\sqrt{2}\phi}{\epsilon} + \frac{\sqrt{2}\epsilon\Delta\phi}{(1-\phi^2)} \\ &= \frac{\sqrt{2}}{\epsilon(\phi^2-1)}\left(\phi^3 - \phi - \epsilon^2\Delta\phi\right) = \frac{\sqrt{2}}{\epsilon(\phi^2-1)}\mu, \end{aligned} \tag{4}$$

where $\mu = \phi^3 - \phi - \epsilon^2\Delta\phi$. Let a regularized Dirac delta function [27] be given as $\delta(\phi) = 3(\phi^2 - 1)^2/\left(4\sqrt{2}\epsilon\right)$, then it satisfies

$$\int_{-\infty}^{\infty}\delta(\phi)\,\mathrm{d}r = \int_{-\infty}^{\infty}\frac{3(\phi^2-1)^2}{4\sqrt{2}\epsilon}\,\mathrm{d}r = 1. \tag{5}$$

We define the elastic bending and surface area energies as

$$W(\phi) = \int_\Omega \kappa H^2\delta(\phi)\,\mathrm{d}\mathbf{x} = \frac{3\kappa}{2\sqrt{2}\epsilon^3}\int_\Omega \mu^2\,\mathrm{d}\mathbf{x}, \tag{6}$$

$$B(\phi) = \int_\Omega \delta(\phi)\,\mathrm{d}\mathbf{x} = \frac{3}{2\sqrt{2}\epsilon}\int_\Omega\left[F(\phi) + \frac{\epsilon^2}{2}|\nabla\phi|^2\right]\mathrm{d}\mathbf{x}. \tag{7}$$

Note that, as ϵ goes to zero, $W(\phi)$ and $B(\phi)$ approaches the bending energy $\mathcal{E}_{\text{elastic}}$ and surface area of Γ, respectively. In addition, the volume is defined as

$$A(\phi) = \int_\Omega \phi(\mathbf{x})\,\mathrm{d}\mathbf{x}. \tag{8}$$

Because $\phi(\mathbf{x})$ is transited from -1 to 1, $A(\phi)$ is not a physical volume, however, it is related by $(A(\phi) + |\Omega|)/2$. To minimize the bending energy W with the constraints for the volume and surface area, we can apply several approaches such as the Lagrange multiplier and penalty methods. Now, we review two numerical methods, the Lagrange multiplier and the penalty methods. Then, we propose a method combined with the Lagrange multiplier and the penalty methods.

2.1. Lagrange multiplier method

The Lagrange multiplier method is a popular method for solving the nonlinear constrained problems. To minimize the bending surface energy $W(\phi)$ with the prescribed volume $A(\phi)$ and surface area $B(\phi)$ constraints, we apply the following gradient flow equation

$$\phi_t = -\frac{\delta W(\phi)}{\delta\phi} - \lambda_1\frac{\delta A(\phi)}{\delta\phi} - \lambda_2\frac{\delta B(\phi)}{\delta\phi}, \tag{9}$$

where $\delta/\delta\phi$ denotes the first variation of the functional and λ_1 and λ_2 are the Lagrange multipliers for the two constraints. Let ϕ be sufficiently smooth and satisfy $\mathbf{n}\cdot\nabla\phi = \mathbf{n}\cdot\nabla\mu = 0$ on $\partial\Omega$. We then have

$$\begin{aligned} \frac{\mathrm{d}}{\mathrm{d}t}W(\phi) &= \frac{\mathrm{d}}{\mathrm{d}t}\left(\frac{3\kappa}{2\sqrt{2}\epsilon^3}\int_\Omega\mu^2\,\mathrm{d}\mathbf{x}\right) = \frac{3\kappa}{\sqrt{2}\epsilon^3}\int_\Omega\mu\left(F''(\phi)\phi_t - \epsilon^2\Delta\phi_t\right)\mathrm{d}\mathbf{x} \\ &= \frac{3\kappa}{\sqrt{2}\epsilon^3}\int_\Omega\left(F''(\phi)\mu - \epsilon^2\Delta\mu\right)\phi_t\,\mathrm{d}\mathbf{x}, \end{aligned} \tag{10}$$

$$\frac{\mathrm{d}}{\mathrm{d}t}A(\phi) = \frac{\mathrm{d}}{\mathrm{d}t}\left(\int_\Omega\phi\,\mathrm{d}\mathbf{x}\right) = \int_\Omega\phi_t\,\mathrm{d}\mathbf{x}, \tag{11}$$

DOI: 10.1002/fld

$$\frac{\mathrm{d}}{\mathrm{d}t}B(\phi) = \frac{\mathrm{d}}{\mathrm{d}t}\left(\frac{3}{2\sqrt{2}\epsilon}\int_\Omega \left[F(\phi) + \frac{\epsilon^2}{2}|\nabla\phi|^2\right]\mathrm{d}\mathbf{x}\right) = \frac{3}{2\sqrt{2}\epsilon}\int_\Omega \mu\phi_t\,\mathrm{d}\mathbf{x}. \tag{12}$$

We identify

$$\frac{\delta W(\phi)}{\delta\phi} := \frac{3\kappa}{\sqrt{2}\epsilon^3}\left(F''(\phi)\mu - \epsilon^2\Delta\mu\right),\ \frac{\delta A(\phi)}{\delta\phi} := 1,\ \text{and}\ \frac{\delta B(\phi)}{\delta\phi} := \frac{3}{2\sqrt{2}\epsilon}\mu.$$

For convenience, let us define $g(\phi) = \delta W(\phi)/\delta\phi$ and $f(\phi) = \delta B(\phi)/\delta\phi$, then we obtain the following governing equation:

$$\phi_t = -g(\phi) - \lambda_1 - \lambda_2 f(\phi). \tag{13}$$

For the volume and surface area conservation, $\int_\Omega \phi_t\,\mathrm{d}\mathbf{x} = 0$ and $\mathrm{d}B(\phi)/\mathrm{d}t = 0$, we have

$$\lambda_1\int_\Omega \mathrm{d}\mathbf{x} + \lambda_2\int_\Omega f(\phi)\,\mathrm{d}\mathbf{x} + \int_\Omega g(\phi)\,\mathrm{d}\mathbf{x} = 0, \tag{14}$$

$$\int_\Omega f(\phi)\left(g(\phi) + \lambda_1 + \lambda_2 f(\phi)\right)\mathrm{d}\mathbf{x} = 0. \tag{15}$$

Lagrange multipliers λ_1 and λ_2 are obtained by solving Eqs. (14) and (15).

2.2. Penalty method

We use two penalty constants M_1 and M_2 to get a modified elastic bending energy as

$$\mathcal{E}_2(\phi) = W(\phi) + M_1(A(\phi) - \alpha)^2 + M_2(B(\phi) - \beta)^2, \tag{16}$$

where α and β are the given volume and surface area, respectively. The solution of the energy minimization can be obtained from the solution of the gradient flow equation

$$\phi_t = -\frac{\delta\mathcal{E}_2(\phi)}{\delta\phi} = -g(\phi) - 2M_1(A(\phi) - \alpha) - 2M_2(B(\phi) - \beta)f(\phi). \tag{17}$$

In general, we should use large penalty constants M_1 and M_2 to enforce the constraints.

2.3. Hybrid method

We propose a hybrid method by combining the penalty and the Lagrange multiplier methods. We modify the original energy equation (16) by ignoring the penalty term for the area $A(\phi)$.

$$\mathcal{E}(\phi) = W(\phi) + M(B(\phi) - \beta)^2. \tag{18}$$

The governing equation can be derived from a constrained gradient flow.

$$\phi_t = -g(\phi) - 2M(B(\phi) - \beta)f(\phi). \tag{19}$$

Because Eq. (19) does not guarantee the volume conservation, we apply the Lagrange multiplier $\gamma(t)F(\phi)$ as

$$\phi_t = -g(\phi) - 2M(B(\phi) - \beta)f(\phi) + \gamma(t)F(\phi), \tag{20}$$

DOI: 10.1002/fld

where $\gamma(t)$ is defined as

$$\gamma(t) = \frac{\int_\Omega [g(\phi) + 2M(B(\phi) - \beta) f(\phi)]\, d\mathbf{x}}{\int_\Omega F(\phi) d\mathbf{x}}. \tag{21}$$

We need to point out that the proposed multiplier is a space–time dependent Lagrange multiplier for the volume constraints; however, it does not guarantee the membrane incompressibility. It is sophisticated to supply the surface area where it is lost from dynamics or numerical calculations.

3. NUMERICAL METHODS

We shall discretize the computational domain $\Omega = (a_1, b_1)\times(a_2, b_2)\times(a_3, b_3)$. Let N_x, N_y, and N_z be the number of cells in the x-direction, y-direction, and z-direction, respectively. And, we assume the uniform mesh with a space step size $h = (b_1 - a_1)/N_x = (b_2 - a_2)/N_y = (b_3 - a_3)/N_z$. The grid points are located at cell-center as

$$\mathbf{x}_{ijk} = (x_i, y_j, z_k) = (a_1 + (i - 0.5)h, a_2 + (j - 0.5)h, a_3 + (k - 0.5)h). \tag{22}$$

We then define the discrete domain as

$$\Omega_h = \left\{\mathbf{x}_{ijk} \mid i = 1, \ldots, N_x, j = 1, \ldots, N_y, k = 1, \ldots, N_z\right\}. \tag{23}$$

Let ϕ^n_{ijk} and μ^n_{ijk} be approximations of $\phi(\mathbf{x}_{ijk}, t_n)$ and $\mu(\mathbf{x}_{ijk}, t_n)$, where $t_n = n\Delta t$ and Δt is a time step. We implement the zero Neumann boundary condition for ϕ by requiring that

$$\begin{aligned} D_x\phi_{-\frac{1}{2},j,k} &= D_x\phi_{N_x+\frac{1}{2},j,k} = D_y\phi_{i,-\frac{1}{2},k} = D_y\phi_{i,N_y+\frac{1}{2},k} \\ &= D_z\phi_{i,j,-\frac{1}{2}} = D_z\phi_{i,j,N_z+\frac{1}{2}} = 0, \end{aligned} \tag{24}$$

where the discrete differential operators are

$$\begin{aligned} D_x\phi_{i+\frac{1}{2},j,k} &= \frac{\phi_{i+1,j,k} - \phi_{ijk}}{h},\ D_y\phi_{i,j+\frac{1}{2},k} = \frac{\phi_{i,j+1,k} - \phi_{ijk}}{h}, \\ \text{and } D_z\phi_{i,j,k+\frac{1}{2}} &= \frac{\phi_{i,j,k+1} - \phi_{ijk}}{h}. \end{aligned} \tag{25}$$

We also implement the Neumann boundary condition for μ in a similar manner. And, we use the notation

$$\nabla_d\phi_{ijk} = \left(D_x\phi_{i+\frac{1}{2},j,k}, D_y\phi_{i,j+\frac{1}{2},k}, D_z\phi_{i,j,k+\frac{1}{2}}\right) \tag{26}$$

to represent the discrete gradient of ϕ at cell-edges. Correspondingly, the divergence at cell-centers, using values at cell-edges, is $\nabla_d \cdot (c, d, e)_{ijk} = D_x c_{ijk} + D_y d_{ijk} + D_x e_{ijk}$. We then define the discrete Laplacian by $\Delta_d\phi_{ijk} = \nabla_d \cdot \nabla_d\phi_{ijk}$. And, we define discrete l_2 inner products by

$$(c, d)_h = h^3 \sum_{i=1}^{N_x}\sum_{j=1}^{N_y}\sum_{k=1}^{N_z} c_{ijk}d_{ijk}, \tag{27}$$

DOI: 10.1002/fld

$$(\nabla_d c, \nabla_d d)_e = h^3 \left(\sum_{i=0}^{N_x} \sum_{j=1}^{N_y} \sum_{k=1}^{N_z} D_x c_{i+\frac{1}{2},j,k} D_x d_{i+\frac{1}{2},j,k} + \sum_{i=1}^{N_x} \sum_{j=0}^{N_y} \sum_{k=1}^{N_z} D_y c_{i,j+\frac{1}{2},k} D_y d_{i,j+\frac{1}{2},k} + \sum_{i=1}^{N_x} \sum_{j=1}^{N_y} \sum_{k=0}^{N_z} D_z c_{i,j,k+\frac{1}{2}} D_z d_{i,j,k+\frac{1}{2}} \right). \tag{28}$$

We also define discrete norms as $\|c\|_2^2 = (c, c)_h$ and $\|\nabla c\|_1^2 = (\nabla_d c, \nabla_d c)_e$.

3.1. Operator splitting method

We use an operator splitting method to solve Eq. (20). We first solve Eq. (19), then adjust the phase-field to recover the volume using the Lagrangian multiplier. Figure 3 illustrates the schematic for the proposed numerical algorithm.

Now, we describe the procedure for the numerical solution from n-th to $(n+1)$-th time step.

Step 1) We discretize Eq. (19) by applying the nonlinearly stabilized splitting scheme [28, 29], which involves a semi-implicit time and centered difference space discretizations as follows:

$$\frac{\phi^*_{ijk} - \phi^n_{ijk}}{\Delta t} = \frac{3\kappa}{\sqrt{2}\epsilon^3} \left(\epsilon^2 \Delta_d \mu^*_{ijk} - F''(\phi^n_{ijk}) \mu^*_{ijk} \right) - \frac{3M \left(B_d(\phi^n) - \beta \right)}{\sqrt{2}\epsilon} \mu^*_{ijk}, \tag{29}$$

$$\mu^*_{ijk} = \left(\phi^*_{ijk} \right)^3 - \phi^n_{ijk} - \epsilon^2 \Delta_d \phi^*_{ijk}, \tag{30}$$

where $B_d(\phi^n) = \frac{3}{2\sqrt{2}\epsilon} \left[(F(\phi^n), \mathbf{1})_h + \frac{\epsilon^2}{2} \|\nabla_d \phi^n\|_1^2 \right]$. We also define discrete energy functionals as

$$W_d(\phi^n) = \frac{3\kappa}{2\sqrt{2}\epsilon^3} \left\| F'(\phi^n) - \epsilon^2 \Delta_d \phi^n \right\|_2^2, \; A_d(\phi^n) = (\phi^n, \mathbf{1})_h \,. \tag{31}$$

We use a nonlinear full approximation storage multigrid method to solve the nonlinear discrete system (29) and (30). To condense the description, we present only the relaxation step for the multigrid method. A detailed description of multigrid method can be found in [30, 31]. First, we rewrite Eqs. (29) and (30) as

$$\begin{aligned} &\frac{\phi^*_{ijk}}{\Delta t} + \left[\frac{3\kappa}{\sqrt{2}\epsilon^3} F'' \left(\phi^n_{ijk} \right) + \frac{9\sqrt{2}\kappa}{\epsilon h^2} + \frac{3M}{\sqrt{2}\epsilon} \left(B_d(\phi^n) - \beta \right) \right] \mu^*_{ijk} \\ &\quad = \frac{\phi^n_{ijk}}{\Delta t} + \frac{3\kappa}{\sqrt{2}\epsilon} \frac{\mu^*_{i+1,jk} + \mu^*_{i-1,jk} + \mu^*_{i,j+1,k} + \mu^*_{i,j-1,k} + \mu^*_{ij,k+1} + \mu^*_{ij,k-1}}{h^2}, \end{aligned} \tag{32}$$

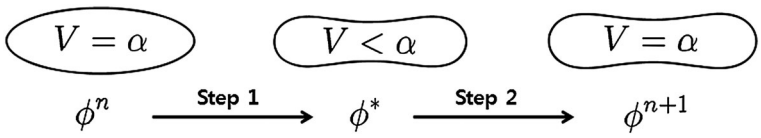

Figure 3. Schematic configurations of the proposed method for one time step. Step 1: reduction of the bending energy with a surface area constraint. Step 2: volume correction.

DOI: 10.1002/fld

$$
\begin{aligned}
&-\left(\phi_{ijk}^{*}\right)^{3}-\frac{6\epsilon^{2}}{h^{2}}\phi_{ijk}^{*}+\mu_{ijk}^{*}\\
&\quad=-\phi_{ijk}^{n}-\epsilon^{2}\frac{\phi_{i+1,jk}^{*}+\phi_{i-1,jk}^{*}+\phi_{i,j+1,k}^{*}+\phi_{i,j-1,k}^{*}+\phi_{ij,k+1}^{*}+\phi_{ij,k-1}^{*}}{h^{2}}.
\end{aligned}
\tag{33}
$$

We linearize the nonlinear term $\left(\phi_{ijk}^{*}\right)^{3}$ with respect to ϕ_{ijk}^{m},that is, $\left(\phi_{ijk}^{*}\right)^{3}=\left(\phi_{ijk}^{m}\right)^{3}+3\left(\phi_{ijk}^{m}\right)^{2}\left(\phi_{ijk}^{*}-\phi_{ijk}^{m}\right)$. After substituting this linearlization into Eq. (33), we obtain

$$
\begin{aligned}
&-\left(3\left(\phi_{ijk}^{m}\right)^{2}+\frac{6\epsilon^{2}}{h^{2}}\right)\phi_{ijk}^{*}+\mu_{ijk}^{*}=-\phi_{ijk}^{n}-2\left(\phi_{ijk}^{m}\right)^{3}\\
&-\epsilon^{2}\frac{\phi_{i+1,jk}^{*}+\phi_{i-1,jk}^{*}+\phi_{i,j+1,k}^{*}+\phi_{i,j-1,k}^{*}+\phi_{ij,k+1}^{*}+\phi_{ij,k-1}^{*}}{h^{2}}.
\end{aligned}
\tag{34}
$$

Step 2) The updated phase-field ϕ_{ijk}^{n+1} is then obtained by

$$
\phi_{ijk}^{n+1}=\phi_{ijk}^{*}+\Delta t\gamma^{*}F\left(\phi_{ijk}^{*}\right),
\tag{35}
$$

where $\gamma^{*}=\left(\phi^{n}-\phi^{*},\mathbf{1}\right)_{h}/\left[\Delta t\left(F(\phi^{*}),\mathbf{1}\right)_{h}\right]$. Hence, the proposed scheme satisfies the volume conservation property by

$$
\left(\phi^{n+1},\mathbf{1}\right)_{h}=\left(\phi^{*},\mathbf{1}\right)_{h}+\Delta t\gamma^{*}\left(F(\phi^{*}),\mathbf{1}\right)_{h}=\left(\phi^{n},\mathbf{1}\right)_{h}.
\tag{36}
$$

3.2. Adaptive method for the surface area constraint

A large fixed number is usually used for the penalty constant M; however, choosing an optimal number is not an easy task, and the surface area $B_d(\phi)$ does not converge to the desired surface area. Thus, we propose an adaptive algorithm for β to converge to the desired surface area β_d.

The main idea of the algorithm is that we adaptively change the value of β by monitoring the tendency of $B_d(\phi)$. First, we define the initial state $\beta^0=\beta_d$. For simplicity, we define the first and second time derivatives as

$$
d_t B_d^{n-1}=\frac{B_d^{n}-B_d^{n-2}}{2\Delta t}\ \text{and}\ d_t^2 B_d^{n-1}=\frac{B_d^{n}-2B_d^{n-1}+B_d^{n-2}}{\Delta t^2}.
\tag{37}
$$

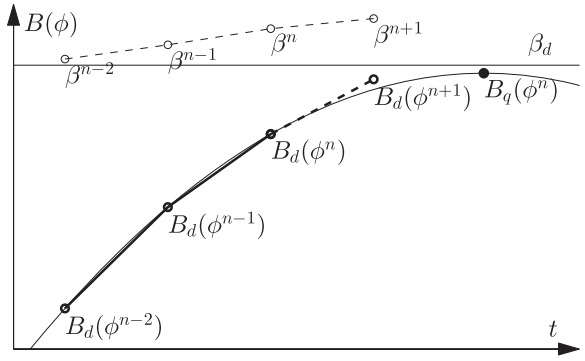

Figure 4. Algorithm for the surface area constraint β^{n+1} at time t_{n+1}.

DOI: 10.1002/fld

We denote B_q^n as the extrema of the quadratic approximation at t_{n-1}. If the condition $d_t B_d^{n-1} \cdot d_t^2 B_d^{n-1} < 0$ holds, then we correct the surface area constraint β^{n+1} as

$$\beta^{n+1} = \beta^n + \frac{1}{1+|\sigma|}\left(\beta_d - B_q^n\right), \tag{38}$$

where $\sigma = \left(B_q^n - B_q^{n-1}\right)/\Delta t$. Otherwise, $\beta^{n+1} = \beta^n$. This proposed algorithm is illustrated in Figure 4. If the condition is positive, we expect that the value of $B_d(\phi)$ could be rapidly changed.

4. NUMERICAL RESULTS

We perform the following numerical experiments: convergence test, evolution of the fluid vesicles, and effects of the penalty constant and surface area constraints. Unless otherwise stated, we use the initial condition as $\phi(\mathbf{x}, 0) = \tanh\left(r/\left(\sqrt{2}\epsilon\right)\right)$, where

$$r = 0.245 - \sqrt{(x-1)^2/8 + (y-1)^2/8 + (z-0.5)^2}. \tag{39}$$

Also, the computational domain is $\Omega = (0,2)\times(0,2)\times(0,1)$, and for other parameters, we use $\kappa = 1, \epsilon = 0.06, h = 1/32$, and $\Delta t =$ 1e-5. Then, the initial volume $A_d(\phi^0)$ and surface area $B_d(\phi^0)$ are -2.757 and 4.415, respectively. We denote the initial volume as $\alpha = A_d(\phi^0)$.

4.1. Convergence tests

The initial condition is $\phi(\mathbf{x}, 0) = \tanh\left(r/\left(\sqrt{2}\epsilon\right)\right)$, where

$$r = 0.35 - \sqrt{(x-1)^2/3 + (y-1)^2/3 + (z-0.5)^2}. \tag{40}$$

To obtain the convergence rates, we perform a number of simulations with increasingly finer grids. The numerical simulations are performed on the uniform grids $h = 1/2^n$ for $n = 4$, 5, and 6. We implement the numerical computation up to time $t =$ 1e-4 with the time step $\Delta t =$ 1e-5. We fix the transition layer $\epsilon = 0.06$ and the interface area constraint $\beta = 5$. The error is defined by the difference between the own grid and interpolation of solution in the twice finer grid

$$\begin{aligned} e_{h_{ijk}} := \phi_{h_{ijk}} - \frac{1}{8}\Big(&\phi_{\frac{h}{2}2i,2j,2k} + \phi_{\frac{h}{2}2i-1,2j,2k} + \phi_{\frac{h}{2}2i,2j-1,2k} + \phi_{\frac{h}{2}2i-1,2j-1,2k} \\ &+ \phi_{\frac{h}{2}2i,2j,2k-1} + \phi_{\frac{h}{2}2i-1,2j,2k-1} + \phi_{\frac{h}{2}2i,2j-1,2k-1} + \phi_{\frac{h}{2}2i-1,2j-1,2k-1}\Big). \end{aligned} \tag{41}$$

By the Richardson method, the convergence rate is defined as a ratio of errors: $\log_2(\|e_h\|_2/\|e_{h/2}\|_2)$. Table I lists the errors and convergence rates. As expected from the discretization, the numerical results show that the scheme has second-order accuracy with respect to space.

Table I. Error norms and convergence rates in space at time $t =$ 1e-4.

h	1/16	Rate	1/32	Rate	1/64
$\|e_h\|_2$	7.003e-3	1.990	1.762e-3	1.998	4.413e-4

DOI: 10.1002/fld

Table II. Error norms and convergence rates in time with $h = 1/32$.

Δt	4e-6	Rate	2e-6	Rate	1e-6
$\|e_{\Delta t}\|_2$	2.220e-3	1.028	1.080e-3	1.013	5.353e-4

To obtain the convergence rate for the time, we simulate with the space step $h = 1/32$ and a set of time steps as $\Delta t =$ 4e-6, 2e-6, and 1e-6. We run the computation up to time $T =$ 4e-4. We define the error as $e_{\Delta t_{ijk}} := \phi_{\Delta t_{ijk}} - \phi_{\Delta t/2_{ijk}}$. Table II lists the errors and convergence rates. We observe first-order accuracy with respect to time, as expected from the discretization.

4.2. *Evolution with the constant surface area constraint*

We consider the evolution of Willmore flow with the constant surface area constraint β to show the limitation of the penalty method. We run the simulation up to $t = 0.03$. For the other parameter, we use the penalty constant $M = 300$, surface area $\beta_d = 5$, and $h = 1/32$. Figure 5(a)–(d) shows the evolution of the surface shape of ϕ. The initial ellipsoid shape becomes to the fluid vesicles. Figure 5(e) shows transverse sections of ϕ at $y = 1$ as time evolves. And Figure 5(f) depicts the normalized volume $A_d(\phi^n)/\alpha$ and surface area $B_d(\phi^n)/\beta_d$. $A_d(\phi^n)/\alpha = 1$ verifies the volume

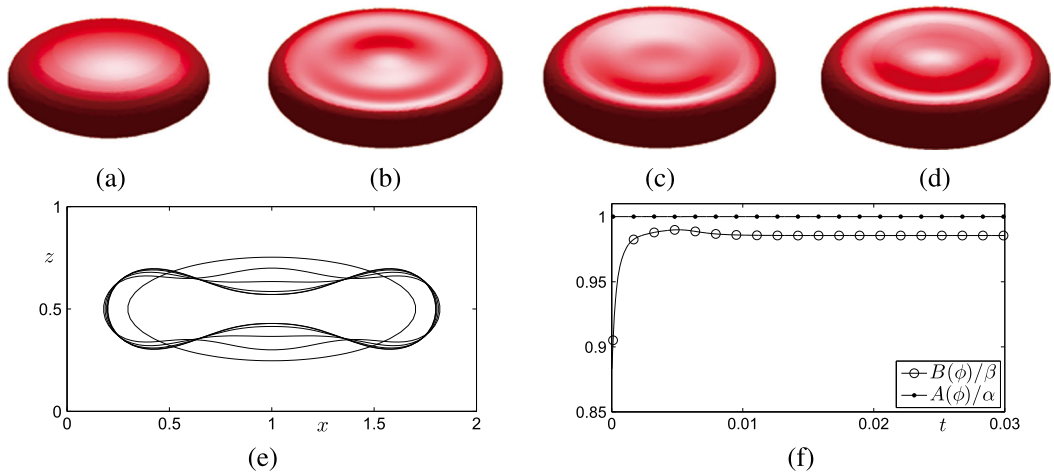

Figure 5. Evolution of the surface shape at time (a) $t = 0$, (b) $t =$ 2e-3, (c) $t =$ 4e-3, and (d) $t =$ 1e-2. (e) Contours at every 200 iterations. (f) Normalized surface area and volume.

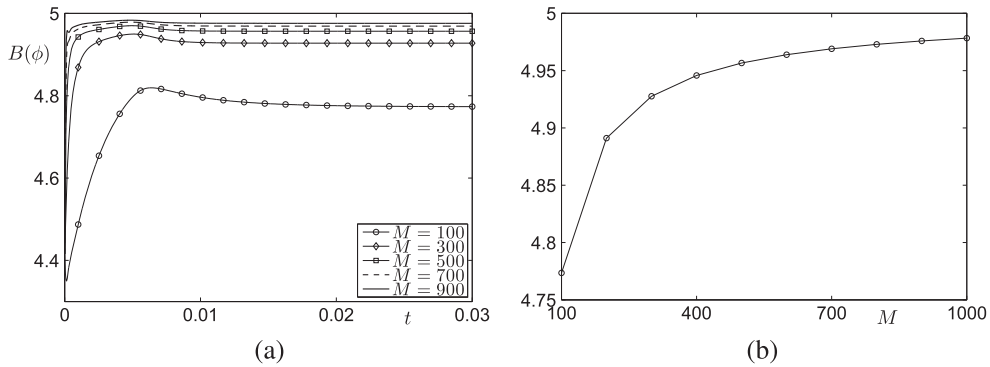

Figure 6. (a) Evolution of the surface area with different penalty values and (b) surface area at time $t = 0.03$ via the different penalty constants.

DOI: 10.1002/fld

conservation of the hybrid scheme. However, $B_d(\phi^n)/\beta$ does not converge to 1, which means that the equilibrium shape does not have the given surface area.

4.3. Penalty constant

We investigate the effect of penalty constant M with the fixed $\beta = 5$. Figure 6(a) shows the evolution of the surface area $B(\phi)$ with different penalty constants M. $B(\phi)$ increases at the earlier stage and converges to some value at the steady state. As M is increased, $B(\phi)$ at the steady-state approaches to 5, as shown in Figure 6(b). However, the numerical method is not stable if we use a more larger value of M.

4.4. Surface area

We consider the effect of surface area β with the fixed $M = 100$. Figure 7(a) shows the evolution of the surface area $B_d(\phi)$ with different surface area values β. The surface area $B_d(\phi)$ increases and then converges to some value at the steady state. As the value of β increases, the surface area $B_d(\phi)$ increases; see Figure 7(b). The dashed line is an expanded line with the first two values, and it infers that the increase of the surface area at the steady state is not linear.

We can expect a value that the surface area at the steady state is 5, and we denote it as β^*. This is a motivation of the proposed adaptive algorithm for the surface area constraint because we can control parameters to obtain a desired surface area.

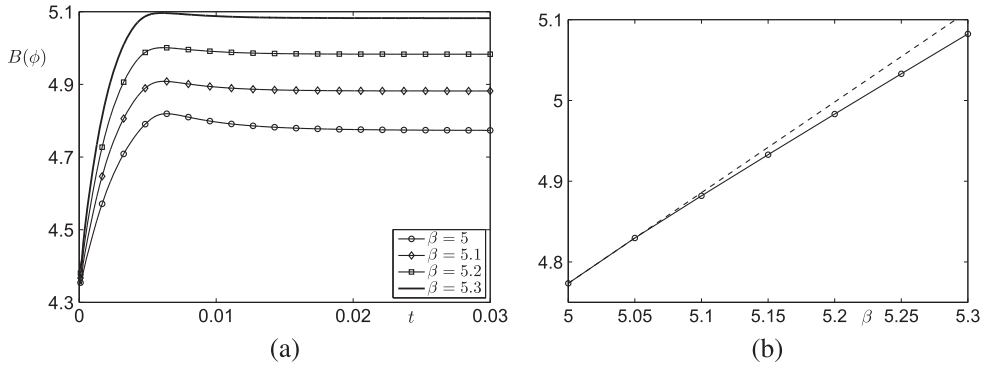

Figure 7. (a) Evolution of the surface area with surface area values and (b) last surface area via the surface area.

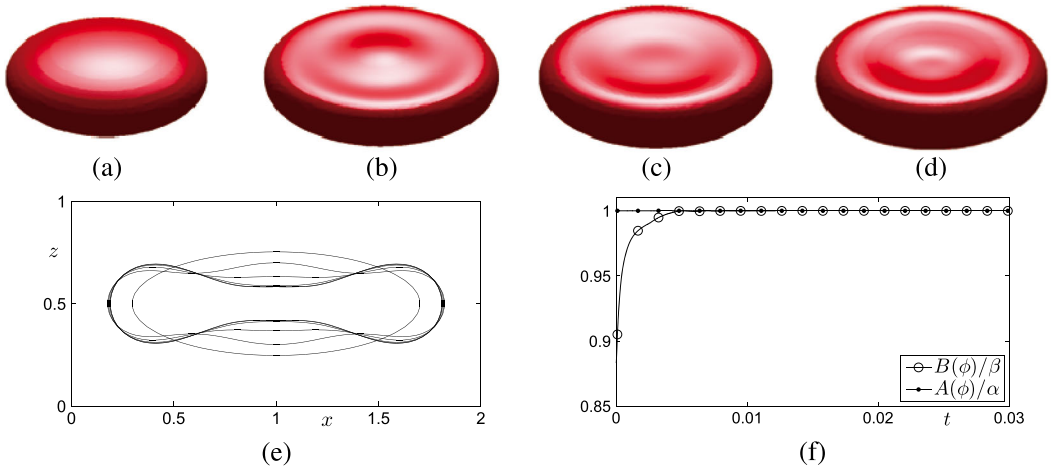

Figure 8. Evolution of the surface shape at time (a) $t = 0$, (b) $t =$ 2e-3, (c) $t =$ 4e-3, and (d) $t =$ 1e-2. (e) Contours at every 200 iterations. (f) Normalized surface area and volume.

DOI: 10.1002/fld

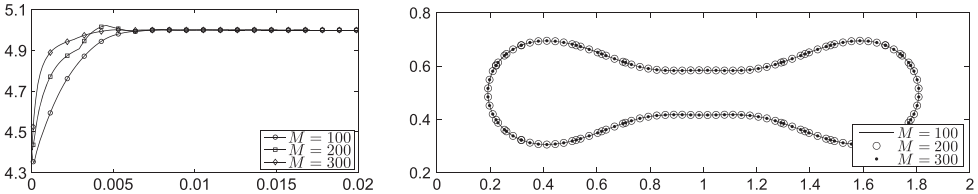

Figure 9. (a) Evolutions of the surface area and (b) contours at the steady state with different penalty constants.

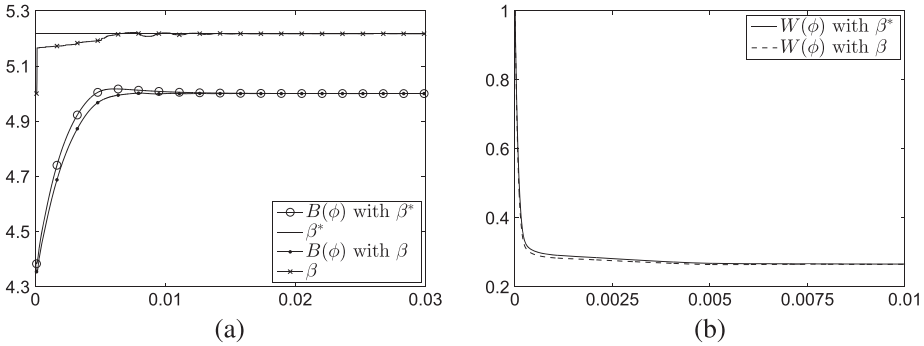

Figure 10. Comparison without and with the variable surface area constraints. (a) Evolutions of the surface areas $B(\phi)$ and constraints β. (b) Bending energy via the time variable.

4.5. Evolution with the variable surface area constraint

We consider the evolution of Willmore flow with the variable surface area constraint. We run the simulation up to $t = 0.03$. For the other parameter, we use the penalty constant $M = 300$ and the surface area $\beta = 5$. Figure 8(a)–(d) shows the evolution of the surface shape of ϕ. An ellipse shape is elongated and it becomes to the fluid vesicles at the steady state. Figure 8(e) shows the zero level contours of ϕ at $y = 1$. And, Figure 8(f) depicts the normalized volume $A_d(\phi^n)/\alpha$ and surface area $B_d(\phi^n)/\beta$. In contrast with Figure 5, $B_d(\phi^n)/\beta$ asymptotically approaches to 1. The evolutions in Figure 8 are similar to those in Figure 5, but the steady-state result with the variable surface area constraints has the given surface area and volume.

4.6. Penalty constants with the variable surface area constraint

Figure 9(a) shows the evolution of the surface area with different penalty constants M. The three evolutions converge to the desired surface area $\beta_d = 5$. The contours at $t = 0.03$ are drawn in Figure 9(b). The adaptive method for the surface area is applied after the first ten iterations.

4.7. Surface area with the variable surface area constraint

We compare the evolution of the surface area without and with the variable surface area constraint; see Figure 10(a). For the constant constraints, we use $\beta = \beta^*$ and $M = 100$. At $t = 0.03$, the difference of the bending energy $W(\phi)$ is 8.24e-4 and that of the surface area constraint is 7.90e-5.

5. CONCLUSIONS

We proposed an accurate and robust numerical method for the phase-field model of a vesicle membrane. The proposed numerical method combines the penalty and the Lagrange multiplier methods for the surface area and volume constraints. The Lagrange multiplier corrects the volume directly, and numerical results demonstrated the volume conservation. We investigate the effect of

DOI: 10.1002/fld

the penalty and constraint values to show the limitation and motivation. The adaptive constraint method for the surface area was presented to resolve the problem that the surface area does not converge to the desired surface area. We demonstrated the accuracy and effectiveness of the proposed numerical method.

ACKNOWLEDGEMENTS

This research was supported by the Basic Science Research Program through the National Research Foundation of Korea (NRF) funded by the Ministry of Education (NRF-2011-0023794). The author (J. Shin) is supported by the Basic Science Research Program through the National Research Foundation of Korea (NRF) funded by the Ministry of Education (2009-0093827). The authors are grateful to the reviewers whose valuable suggestions and comments significantly improved the quality of this paper.

REFERENCES

1. McMahon HT, Gallop JL. Membrane curvature and mechanisms of dynamcis cell membrane remodelling. *Nature* 2005; **438**:590–596.
2. Seifert U. Configurations of fluid membranes and vesicles. *Advances in Physics* 1997; **46**:13–137.
3. Döbereiner H, Evans E, Kraus M, Seifert U, Wortis M. Mapping vesicle shapes into the phase diagram: a comparison of experiment and theory. *Physical Review E* 1997; **55**:4458–4474.
4. Evans E, Needham D. Physical properties of surfactant bilayer membranes: thermal transitions, elasticity, rigidity, cohesion, and colloidal interactions. *Journal of Chemical Physics* 1987; **91**:4219–4228.
5. LePesant JP, Powers L, Pershan PS. Brillouin light scattering measurement of the elastic properties of aligned multilamella lipid samples. *Proceedings of the National Academy of Sciences* 1978; **75**:1792–1795.
6. Evans E, Fung YC. Improved measurements of erythrocyte geometry. *Microvascular Research* 1972; **4**:335–347.
7. Ou-Yang ZC, Helfrich W. Instability and deformation of a spherical vesicle by pressure. *Physical Review Letters* 1987; **59.21**:2486.
8. Du Q, Liu C, Wang XQ. A phase field approach in the numerical study of the elastic bending energy for vesicle membranes. *Journal of Computational Physics* 2004; **198**:450–468.
9. Du Q, Liu C, Ryham R, Wang XQ. A phase field formulation of the Willmore problem. *Nonlinearity* 2005; **18**: 1249–1267.
10. Du Q, Liu C, Wang XQ. Simulating the deformation of vesicle membranes under elastic bending energy in three dimensions. *Journal of Computational Physics* 2006; **212**:757–777.
11. Biben T, Misbah C. Tumbling of vesicles under shear flow within an advected-field approach. *Physical Review E* 2003; **67**:031908-1–031908-5.
12. Biben T, Kassner K, Misbah C. Phase-field approach to three-dimensional vesicle dynamics. *Physical Review E* 2005; **72**:041921-1–041921-15.
13. Du Q, Li M, Liu C. Analysis of a phase field Navier–Stokes vesicle-fluid interaction model. *Discrete and Continuous Dynamical Systems - Series B* 2007; **8**:539–556.
14. Kraus M, Wintz W, Seifert U, Lipowsky R. Fluid vesicles in shear flow. *Physical Review Letters* 1996; **77**:3685.
15. Gompper G, Kroll DM. Network models of fluid, hexatic and polymerized membranes. *Journal of Physics: Condensed Matter* 1997; **9**:8795.
16. Noguchi H, Gompper G. Fluid vesicles with viscous membranes in shear flow. *Physical Review Letters* 2004; **93**:258102.
17. Noguchi H, Gompper G. Shape transitions of fluid vesicles and red blood cells in capillary flows. *Proceedings of the National Academy of Sciences of the United States of America* 2005; **102**:14159–14164.
18. Pivkin IV, Karniadakis GE. Accurate coarse-grained modeling of red blood cells. *Physical Review Letters* 2008; **101**:118105.
19. Du Q, Zhang C. Adaptive finite element method for a phase field bending elasticity model of vesicle membrane deformations. *SIAM Journal on Scientific Computing* 2007; **30**:1634–1657.
20. Ou-Yang ZC, Helfrich W. Bending energy of vesicle membranes: general expressions for the first, second and third variation of the shape energy and applications to spheres and cylinders. *Physical Review E* 1989; **39**:5280–5288.
21. Campelo F, Hernández-Machado A. Dynamic model and stationary shapes of fluid vesicles. *The European Physical Journal E* 2006; **20**:37–45.
22. Seifert U. Adhesion of vesicles in two dimensions. *Physical Review A* 1991; **43**:6803–6814.
23. Seifert U. Curvature-induced lateral phase segregation in two-component vesicles. *Physical Review Letters* 1993; **70**:1335–1338.
24. Lowengrub JS, Rätz A, Voigt A. Phase-field modeling of the dynamics of multicomponent vesicles: spinodal decomposition, coarsening, budding, and fission. *Physical Review E* 2009; **79**:0319261-1–0319261-13.
25. Ciarlet PG. *Mathematical Elasticity: Three-dimensional Elasticity*, Vol. 29. Springer: North-Holland, 2000.

DOI: 10.1002/fld

26. Ou-Yang ZC, Liu JX, Xie YZ. *Geometric Methods in the Elastic Theory of Membranes in Liquid Crystal Phases*. No.2 World Scientific: Singapore, 1999.
27. Lee HG, Kim J. Regularized Dirac delta functions for phase-field models. *International Journal for Numerical Methods in Engineering* 2012; **91**:269–288.
28. Eyre DJ. Unconditionally gradient stable time marching the Cahn–Hilliard equation. In Materials Research Society Symposium Proceedings. *The Material Research Society* 1998; **529**:39–46.
29. Kim JS, Bae HO. An unconditionally gradient stable adaptive mesh refinement for the Cahn–Hilliard equation. *Journal of the Korean Physical Society* 2008; **53**:672–679.
30. Briggs WL. *A Multigrid Tutorial*. SIAM: Philadelphia, 1987.
31. Trottenberg U, Oosterlee CW, Schüller A. *Multigrid*. Academic Press: London, 2001.

DOI: 10.1002/fld